HAIT Journal of Science and Engineering, Volume 1, Issue 4, pp. 721-742

Fast phase transition and shock waves of the vortex matter in type-II superconductors *

Boris Ya. Shapiro[1,*], Irina Shapiro[1],
Baruch Rosenstein[2], and Pei Jen Lin[2]

[1] *Department of Physics, Bar Ilan University, Ramat Gan 52100, Israel*
[2] *Department of Electrophysics, National Chiao Tung University, Hsinchu, Taiwan, R.O.C.*
[*] *Corresponding author: shapib@mail.biu.ac.il*
Received 7 December 2004, accepted 25 March 2005

Abstract

The relaxation dynamics of a quenched normal domain in a type-II superconductor is considered analytically and numerically. Different instabilities accompanying recovery of superconductivity are predicted. The relaxation of the normal spot starts with appearance of a microscopic instability leading to emergence of the vortex clusters. Effects of the heat dissipation and transport on the motion and stability of the interface between the magnetic flux and flux-free domains are considered. It is shown that the magnetic induction and the temperature profiles have a form of the shock wave moving with a constant velocity. In the vicinity of the front, superconductivity is suppressed by strong screening currents. The front velocity is determined completely by the Joule heat caused by electric current in the normal domain at the flux front. Stability of the shock wave solution is investigated both analytically and numerically. For sufficiently small heat diffusion constant, a finger-shaped thermal instability is found.

PACS: 74.20.De, 74.60.Ge

[*]Presented at Research Workshop of the Israel Science Foundation *Correlated Electrons at High Magnetic Fields*, Ein-Gedi/Holon, Israel, 19-23 December 2004

Introduction

The dynamics of magnetic flux penetration into type II superconductor and its instabilities has been studied by variety of techniques over the years (see [1] and references therein). Magneto-optical experiments [2] demonstrate that in a wide range of situations there exists a well defined interface (front) between the magnetic flux penetrating a sample and the flux free Meissner state. Magneto-optical technique has been further perfected and revealed a wide class of instabilities, including magnetic macro-turbulence, [3], dendritic instability [4]. The instability of the magnetic flux and flux avalanches are observed both in anisotropic HTSC [3] and in an isotropic material like Nb [4].

Recently, a new type of flux instability has been observed experimentally. In this experiments superconductivity was locally destroyed in a completely nonadiabatic fashion by a femtosecond laser pulse [5]. The pulse clearly forces the system out of thermal equilibrium. Superconductivity is destroyed inside a narrow stripe of the YBCO film subjected to magnetic field perpendicular to the film. The field does not exceed the first critical field H_{c1}, so that initially fluxons cannot penetrate the rest of the sample. Therefore the magnetic flux initially fills the normal domain. Recovery of superconductivity occurs in two stages. After the short pulse has past, the stripe is cooled, and the flux nucleates into a dense system of Abrikosov vortices. The microscopic characteristic time of that stage is of order of the Ginzburg-Landau relaxation time (appearing in the time dependent GL equations) $t_{GL} \sim 10^{-10}\,\mathrm{sec}$. On the larger (mesoscopic) time scale the rapidly created vortices are pushed into the superconducting part of the sample. The fluxons move very fast with velocities of order of 10^5cm/sec in YBCO [5]. The flux flow currents J in this case are much higher than the critical current J_c typical for the thermodynamic Bean critical state, but smaller (although not much smaller) than the depairing current J_d: $J_d > J >> J_c$. Just after the vortex nucleation stage, the magnetic flux forms a rapidly moving front. This highly nonequilibrium relaxation dynamics is very different from the essentially adiabatic dynamics of the critical state. The front line shape is not always stable: sometimes it dynamically develops the dendritic-like structures [6]. It is interesting that the dendrites appear at well separated points indicating that certain threshold has been crossed.

In the present paper, we first review a recent progress in understanding the rapid relaxation of unstable normal state and subsequent creation of dynamic vortex domain. A major theoretical tool is direct simulation of the time dependent GL equations appropriate for the microscopic time scale of

these processes. Then we use the numerical and analytical analysis of the flux hydrodynamics to study the motion and stability of the flux domain on the mesoscopic time scale. For certain voltage-current characteristics of the superconductor in its resistive state, the magnetic induction penetrating a flux free superconductor forms a sharp front. The Joule heat released at the flux front can provide constant velocity of the front propagation inside the type II superconductors. The straight front line shows instability with respect to local temperature fluctuations. In fact, an excessive local temperature at the front leads to excessive Joule heat released there and, in turn, increases the local front velocity in the fluctuation area. The hydrodynamical tangential instability of the flux front destroys the flat front.

1 Fast phase transition and creation of the vortex domain

We start with the simplified set of the time-dependent Ginzburg-Landau (TDGL) equations coupled with the temperature diffusion equation. The TDGL equations, being exact in gapless superconductors, are known to provide a qualitatively correct description in other cases. We consider the temperature diffusion equation in the local temperature approximation. This model describes superconductors, where the energy relaxation time is about 10^{-13} sec and the electron subsystem returns rapidly to the equilibrium, while the ion subsystem relaxes relatively slowly to the temperature of the environment (in other words, the characteristic ion relaxation time $t_h \geq \tau_{GL} \sim 10^{-11}$ sec). The temperature of the ion subsystem in this approximation can be treated as a local one, $T = T(\mathbf{r},t)$.

Choosing the scalar potential in the form $\mu = -\partial\chi/\partial t$, we can rewrite the TDGL equations in a dimensionless form:

$$\Gamma\frac{\partial\psi}{\partial t} = (1-\Theta(\mathbf{r},t))\psi - |\psi|^2\psi - (i\boldsymbol{\nabla}+\mathbf{A})^2\psi \tag{1}$$

$$\frac{\partial\mathbf{A}}{\partial t} = -\boldsymbol{\nabla}\times\boldsymbol{\nabla}\times\mathbf{A} - \frac{i}{2\kappa^2}(\psi^*\boldsymbol{\nabla}\psi - \psi\boldsymbol{\nabla}\psi^*) - \frac{1}{\kappa^2}|\psi|^2\mathbf{A} \tag{2}$$

$$\frac{\partial\Theta}{\partial t} = \varkappa\boldsymbol{\nabla}^2\Theta + \nu(\frac{\partial\mathbf{A}}{\partial t})^2 - \gamma(\Theta-\Theta_0) \tag{3}$$

$$\psi(\mathbf{r},t) = |\psi(\mathbf{r},t)|\exp(i\chi(\boldsymbol{\rho},t)). \tag{4}$$

It should be noted that in the general case these equations are three-dimensional, but for thin samples when $L \approx \delta$ (here L and δ are the thickness of the

sample and the penetration depth of the magnetic field, respectively) they reduce to the two-dimensional modified TDGL equations.

The dimensionless variables are related to the dimensional ones as follows:

$$r = r^{'}/\xi, \quad t = t^{'}/\tau_{GL}\,, \quad \tau_{GL} = 4\pi\sigma\xi^2/c^2, \quad \nu = \kappa^2 H_{cm}^2/2\pi T_c C_v, \qquad (5)$$

$$\mathbf{A} = \mathbf{A}^{'}/\left(\sqrt{2}\delta H_{cm}\right), \quad \mathbf{H} = \mathbf{H}^{'}/\left(\sqrt{2}H_{cm}\right), \quad \mu = \frac{8\pi e\sigma\xi^2}{\hbar c^2}\mu^{'}. \qquad (6)$$

In addition, $\Theta(\mathbf{r},t) = T(\mathbf{r},t)/T_c$ is the reduced temperature, $\Theta_0 = T_0/T_c$, where $T_0 < T_c$ is the equilibrium temperature of the superconductor, $\psi = \Psi/\psi_0$ is the dimensionless order parameter (here ψ_0 is the equilibrium magnitude of the order parameter), $\varkappa = \tau_{GL}D(T)/\xi^2$ is the reduced diffusion coefficient, γ is the dimensionless relaxation coefficient, $\kappa = \delta/\xi$ is the Ginzburg-Landau parameter, D is the heat conductivity, $\Gamma = \gamma_{GL}c^2 m/\pi\hbar^2\sigma$, m is the electron mass, C_v is the heat capacity, σ is the conductivity in the normal state, $\gamma_{GL} \sim \hbar\alpha/T_c$ is the characteristic relaxation time of the order parameter, and H_{cm} is the thermodynamic critical magnetic field. The boundary condition for the order parameter is $(i\nabla + \mathbf{A})_n \psi = 0$. The set of equations was solved in thick film geometry where superconductivity was initially destroyed in a narrow strip (Fig. 1) under magnetic field smaller than H_{c1}.

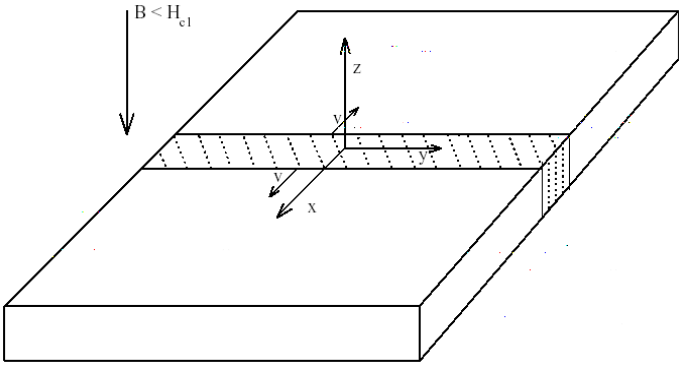

Figure 1: Geometry of the problem. The shaded area contains the flux that penetrated the sample during short initial period when the superconductivity was destroyed at the center ($x = 0$). Arrows indicate the direction of the flux front motion. Direction of the magnetic field B is perpendicular to the xy plane.

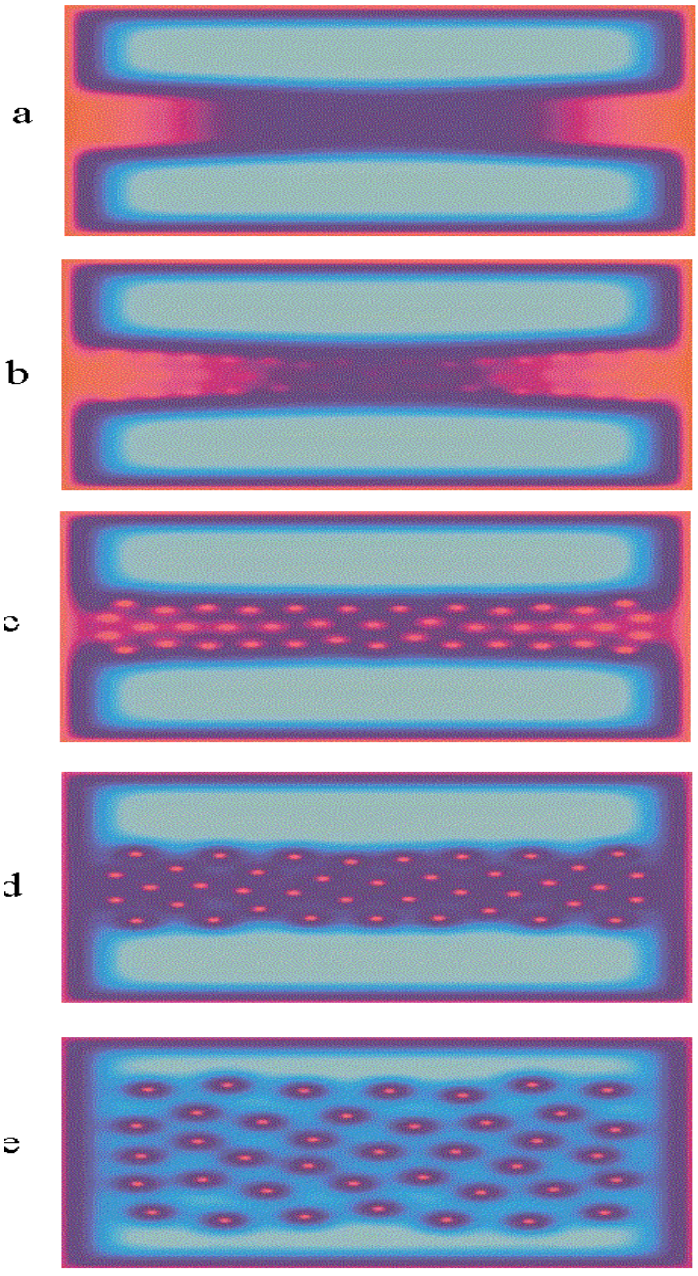

Figure 2: Formation of the vortex domain on the microscopic time scale (in units of the GL time τ_{GL}): a) 0, b) 10^3, c) $2 \cdot 10^3$, d) $4 \cdot 10^3$, e) $6 \cdot 10^3$.

The system was simulated for $H' = 0.5H_{c1}$, $\gamma = 10^{-5}$, and $\kappa = 10$. The results presented in Fig. 2 show the process of the magnetic flux penetration of the laser heated normal strip (Fig. 2a,b) with subsequent formation and development of the quantized fluxons and their organization into the vortex cluster (Figs. 2c-2e). The vortex cluster, however, is unstable since vortices attempt to escape the sample. The boundary of the vortex cluster is typically straight.

2 Dynamics on the mesoscopic time scale

2.1 Hydrodynamics of the vortex matter

The two dimensional vortex matter in the hydrodynamics approximation is described by the magnetic induction $B(\mathbf{r}, t)$ and the temperature profile $T(\mathbf{r}, t)$, where $\mathbf{r} =(x, y)$ is a two dimensional vector. The basic equations are the Maxwell equation

$$\frac{4\pi}{c^2}\frac{\partial B}{\partial t} = \frac{\partial}{\partial x}\left[R\frac{\partial B}{\partial x}\right] + \frac{\partial}{\partial y}\left[R\frac{\partial B}{\partial y}\right] \tag{7}$$

where resistivity $R(B, T)$ will be phenomenologically defined in the next subsection, and the heat transport equation:

$$C\frac{\partial T}{\partial t} = D\boldsymbol{\nabla}^2 T + \mathbf{J}\cdot\mathbf{E}(B, T) - \gamma C(T - T_0). \tag{8}$$

Here $\gamma_H = 1/t_r$ is the heat relaxation constant with t_r being the heat relaxation time. The first term on the right hand side is the heat conduction, the second is the Joule heat and the third describes the heat exchange between the slab and the cooling liquid. The Joule heat term consists of two different contributions. In the mixed state it is dominated by the motion of the magnetic flux, while in the normal metal when the superconductivity is suppressed by the currents, one has usual Ohmic resistance losses.

2.2 Resistivity at high currents

As a rule, the nonlinear resistivity $R\left(J, B, T\right) \equiv E\left(J, B, T\right)/J$ in the mixed state of a type II superconductor is a complicated function of magnetic field, current, and temperature, see Fig. 3. In this work we will be interested mainly in resistivity at currents much larger than the critical current J_c, when the pinned vortices are released. The vortex resistivity grows quickly above J_c, either exponentially or as a power $R \propto J^{\mu}$ with large μ. In this

relatively low current regime the dependence on magnetic induction B is very weak. However, when the current approaches the depairing current J_d, the power μ becomes smaller and resistivity strongly depends on B. Recently detailed measurements of the $I-V$ characteristics of Nb films at high current density of order 10^6 A/cm^2 were performed [7]. Near the depairing current it has a form

$$R(B,T) = R_n(T)\left(\frac{J}{J^*(T,B)}\right)^{\mu} . \tag{9}$$

Here $R_n(T)$ is the normal state resistivity. The depairing current J^* dependence on magnetic field and temperature [7] can be fitted well by the following form:

$$J^*(T,B) = J_d\Delta\left(\frac{B_{c2}(T)}{B}\right)^{\nu/\mu} . \tag{10}$$

The upper critical field depends on temperature as $B_{c2}(T) = B_{c2}(0)\Delta$, where we assumed that dimensionless temperature $\theta = T/T_c$ is not far from 1, namely $\Delta \equiv 1-\theta$ is small. When the current exceeds $J^*(B,T)$, the electric field is continuous, the resistivity approaching its normal value $R(B,T) = R_n(T)$. Thus the nonlinear flux diffusion equation Eq. (7) contains a derivative of R which is a discontinuous function.

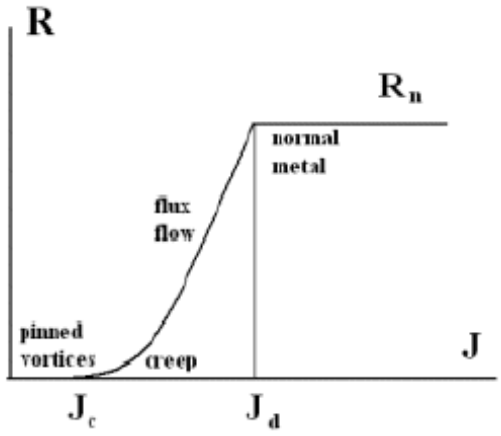

Figure 3: Schematic plot of the nonlinear resistivity of the type-II superconductor in the mixed state as a function of the current. The resistivity is zero below the critical current J_c , exponentially small in the flux creep regime just above J_c and evolves into a power function in the flux flow regime. At the depairing current it merges with ohmic normal state resistivity.

We fitted the $I-V$ curves of Nb and obtained $\mu = 1.5$ with temperature independent R_n. For Nb at fields of the order of B_{c1}, we obtain the best fit $\nu = 1.3$. The values of other material parameters are: $B_{c2}(0) = 4.43$ **T**, $R_n = 9.9$ $\mu\Omega$·cm and $T_c = 8.6$ K. These were measured directly. The best fit is obtained for the constant $J_d = 9.2 \cdot 10^6$ A/cm^2. (see Fig. 4 for a sample of data taken at $T = 7.8$ K, $\theta = 0.9$). Of course, the exponents depend on material and weakly depend on field for larger magnetic fields. The power law, however, generally holds.

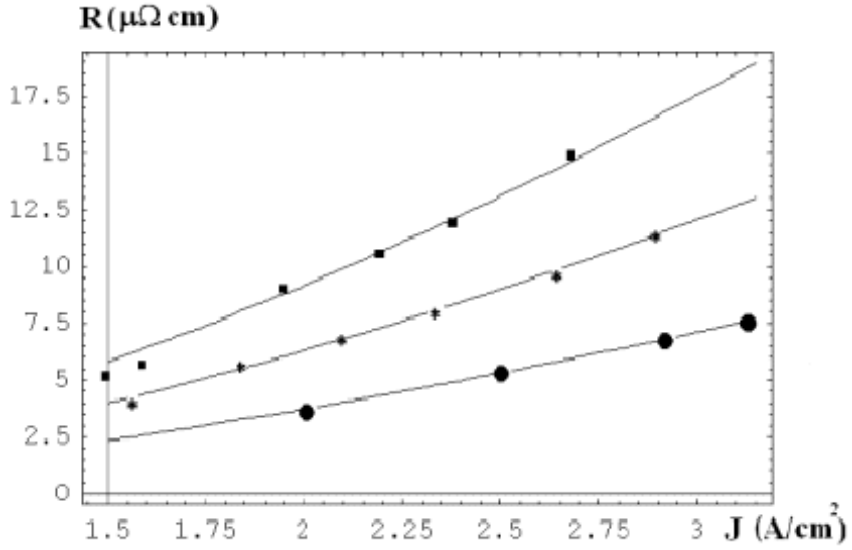

Figure 4: Fitting the resistivity dependence on the current density of [7] with our model resistivity Eqs. (9)-(10) with $\nu = 1.3$, $\mu = 1.5$. Magnetic field is 20 mT (circles), 30 mT (stars) and 40 mT (squares).

2.3 Basic equations in terms of dimensionless quantities

Dimensionless coordinate, time, and magnetic induction are defined using the natural units of length $x^* = cR_n(T = T_c) \equiv cR_n$, magnetic field $B^* = \sqrt{4\pi C T_c}$ and time $x \to x/x^*; \qquad t \to t/t^*; \qquad b = B/B^*$.

$$t^* = 4\pi R_n \left(\frac{4\pi R_n J_d}{B^*}\right)^{\mu} \left(\frac{B_{c2}\,(0)}{B^*}\right)^{\nu}; B^* \approx H_{c1}\frac{\lambda^2 k_F v_F}{c\xi} \tag{11}$$

The set of nonlinear coupled equations in the superconducting state ($J < J^*(B,T)$) reads:

$$\frac{\partial b}{\partial t} = \frac{\partial}{\partial x}\left(\rho\frac{\partial b}{\partial x}\right) + \frac{\partial}{\partial y}\left(\rho\frac{\partial b}{\partial y}\right) \tag{12}$$

$$\frac{\partial \theta}{\partial t} = \kappa\boldsymbol{\nabla}^2\theta + \rho j^2 - \Gamma(\theta - \theta_0), \tag{13}$$

where the dimensionless resistivity and the electric current density are:

$$\rho = \frac{R_n(\theta)}{R_n}\left(\frac{b}{\Delta}\right)^{\nu}\left(\frac{j}{\Delta}\right)^{\mu} \;\; ; \quad j = \sqrt{\left(\frac{\partial b}{\partial x}\right)^2 + \left(\frac{\partial b}{\partial y}\right)^2}. \tag{14}$$

The flux diffusion equation does not contain parameters, while the heat transfer equation has two of them: the dimensionless temperature diffusion constant and the relaxation coefficient

$$\kappa = \frac{Dt^*}{Cx^{*2}}, \quad \Gamma = \gamma t^*. \tag{15}$$

In the region in which superconductivity is suppressed by the superconducting current J exceeding the depairing current value $J_d(B,T)$, the normal state resistivity becomes $R = R_n(T)$. The dimensionless normal state resistance is defined by $\rho_{_n}(\theta) = R_n(\theta)c^2t^*/4\pi x^{*2}$. In this case the basic equations are

$$\frac{\partial b}{\partial t} = \frac{\partial}{\partial x}\left(\rho_n\frac{\partial b}{\partial x}\right) + \frac{\partial}{\partial y}\left(\rho_n\frac{\partial b}{\partial y}\right) \tag{16}$$

$$\frac{\partial \theta}{\partial t} = \kappa\boldsymbol{\nabla}^2\theta + \rho_n j^2 - \Gamma(\theta - \theta_0). \tag{17}$$

In the following section we solve these equations both analytically and numerically.

3 Structure and evolution of the flux front

3.1 Asymptotics of the straight flux front in the superconducting phase

When the boundary conditions are independent of y , the front is straight and the problem becomes one-dimensional. We start with a case when the resistivity depends only on magnetic induction, hence now we consider $\mu = 0$. In addition, we initially solve a simplified set dropping the relaxation term $\Gamma = 0$ and diffusion $\kappa = 0$. This assumption will be supported *aposteriori*

by calculating the term's effects and comparing with the numerical solution. Looking for the solution of Eqs.(12) and (13) in the form

$$b = b_s(X),\ \Delta = \Delta_s(X), \tag{18}$$

where $X = x - Vt$ is the distance from the interface and V is the interface velocity, one obtains

$$-V\frac{db_s}{dX} = \frac{d}{dX}\left[\left(\frac{b_s}{\Delta_s}\right)^{\nu}\frac{db_s}{dX}\right]. \tag{19}$$

$$V\frac{d\Delta_s}{dX} = P_J. \tag{20}$$

Here the Joule power density is $P_J = \rho\, j^2$. Let us first investigate asymptotics of $b_s(X)$ in the vicinity of the front $X \to 0$. In the cold superconductor magnetic field vanishes. Therefore formally (ignoring formation of the very narrow normal stripe near the front which will be discussed in the next subsection) we look at the magnetic field $b_s(X)$ as the power with some coefficient dependent on velocity only for $X < 0$:

$$b_s(X) = A(V)\,|X|^{\alpha}\,. \tag{21}$$

The temperature is sought off the form:

$$\Delta_s(X) = \Delta_{s0} - \Delta_{s1}(V)\,|X|^{\beta}\,. \tag{22}$$

Substituting the Ansatz Eqs.(21) and (22) into Eqs.(19) and (20), one obtains on the superconducting side of the front ($X < 0$):

$$VA\alpha\,|X|^{\alpha-1} = A^{\nu+1}\Delta_{s0}^{-\nu}\alpha[(\nu+1)\alpha - 1]\,|X|^{(\nu+1)\alpha-2}\,; \tag{23}$$

$$A^{2+\nu}\alpha\,|X|^{2\alpha-2+\alpha\nu} = \Delta_{s1}\beta\Delta_{s0}^{\nu}V\,|X|^{\beta-1}\,, \tag{24}$$

which is satisfied for

$$\alpha = 1/\nu;\ \beta = 2/\nu; \tag{25}$$

$$A(V) = \Delta_{s0}(\nu V)^{1/\nu};\ \Delta_{s1}(V) = \frac{1}{2}\Delta_{s0}^2(\nu V)^{2/\nu}. \tag{26}$$

The electric current $j = \partial b_s/\partial X$ formally diverges as $|X|^{1/\nu-1}$ at the front for $\nu > 1$. Of course, the divergence is intercepted by the phase transition into the normal state creating the "hot" region of presumably small width w_n determined by the condition that depairing current is reached

$$j(X = -w_n) = j_d = \Delta_{s0}V(\nu V w_n)^{1/\nu-1}. \tag{27}$$

There is also dissipation in the superconducting part of a larger width w_s.The expression for the Joule heat term caused by the magnetic flux motion everywhere, not necessarily close to the front interface, diverges at the front as (see Eq.(21)) $P_J \propto |X|^{2/\nu-1}$ for $\nu > 2$ only. Its integral, however, always converges. To determine V, w_n, and other characteristics of the front motion we need the solution in the normal domain. This and its matching with the asymptotics in the superconductor is considered next.

3.2 Solution in the normal domain for the temperature independent resistivity

In the normal domain we assume first for simplicity that $\rho_n(T) = \text{const}$ in addition to the previously used simplification $\kappa = \Gamma = 0$. The nonlinear wave Ansatz

$$b = b_n(X),\ \Delta = \Delta_n(X) \tag{28}$$

will be initially used to find the current density $j_n = \frac{db_n}{dX}$. Substitution of Eq.(28) into the normal state equations (16) and (17) leads to the following set in terms of the front variable $X = x - Vt$:

$$-Vj_n = \rho_n \frac{dj_n}{dX} \tag{29}$$

$$V\frac{d\Delta_n}{dX} = \rho_n j_n^2. \tag{30}$$

The first equation has a solution

$$j_n(X) = j_{n0} \exp\left[-\frac{XV}{\rho_n}\right] \approx j_{n0}\left(1 - \frac{XV}{\rho_n}\right). \tag{31}$$

The approximate form is generally valid since $\frac{|X|V}{\rho_n} < \frac{w_n V}{\rho_n} \ll 1$ as will be justified *aposteriori.* Then the heat transfer equation and the boundary condition $\Delta_n(X = 0) = \Delta_0$ give

$$\Delta_n(X) = \Delta_0 - \frac{\rho_n j_{n0}^2}{2V^2}\left\{\exp\left[-\frac{2XV}{\rho_n}\right] - 1\right\} \approx \Delta_0 + \frac{j_{n0}^2}{V}X. \tag{32}$$

In this region most of the heat is released

$$\Xi_n \equiv \int\limits_{-w_n}^{0} \rho_n(\theta)\left(\frac{\partial b_n}{\partial X}\right)^2 dX \approx \rho_n j_n^2 w_n. \tag{33}$$

We will use this result below.

3.3 Matching solutions on the superconductor - normal interface and the flux front velocity

The current, temperature, and the temperature gradient are all continuous on the superconductor - normal interface $X = -w_n$. Consequently, the current on the normal side approaches the same depairing current on the superconducting side

$$j_n\left(X = -w_n\right) = j_d = \Delta_{s0} V (\nu V w_n)^{1/\nu - 1}. \tag{34}$$

The temperature matching conditions are

$$\Delta\left(-w_n\right) = \Delta_0 - \frac{j_d^2 w_n}{V} = \Delta_{s0}; \tag{35}$$

$$\Delta'\left(-w_n\right) = \frac{j_d^2}{V} = \frac{\Delta_{s0}^2}{\nu w_n} (\nu V w_n)^{2/\nu}. \tag{36}$$

The only solution of the set of three algebraic equations Eq.(27), Eq.(35), and Eq.(36) is very simple:

$$V = \frac{j_d}{2\Delta_0}\left[1 + \sqrt{1 + 4\Delta_0/\nu}\right] \approx \frac{j_d}{\Delta_0}\left(1 + \frac{\Delta_0}{\nu}\right) \tag{37}$$

where $w_n \approx \Delta_0/\nu j_d, \Delta_{s0} \approx \Delta_0 - \Delta_0^2/\nu$. The front velocity can be represented via the Joule heat released in the normal domain Eq.(33)

$$\Xi_n = \rho_n j_n^2 w_n = \frac{\rho_n j_d \Delta_0}{\nu} \tag{38}$$

as:

$$V = \frac{\nu \Xi_n}{\rho_n \Delta_0^2}. \tag{39}$$

We will use this simple relation in numerical simulation described in the next subsection. As we discuss later, the numerical results demonstrate that the width of the normal domain w_n (hatched area in Fig. 5) is much smaller than the width of the superconducting domain w_s in which the current is significant. When κ and Γ are nonzero only numerical analysis is possible. The results (see below) show that for reasonable values of κ and Γ the corresponding terms in the heat transfer equation are qualitatively insignificant. Of course in this case we cannot assume the simple form of Eq. (18).

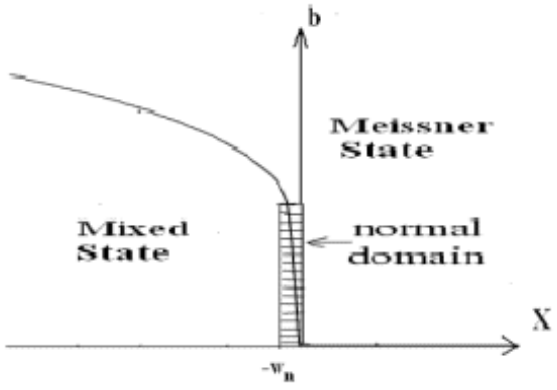

Figure 5: Magnetic induction profile at the front. Three different regions, the mixed, the normal domain, and the Meissner state are presented. Here w_n is the width of the normal domain in which the superconductivity is suppressed by excessive current, shown by the hatched area at the front onset.

3.4 Numerical solution

The set of the scaled one-dimensional equations Eq.(12) and Eq.(13) for resistivity in the form of Eq.(14) in the superconducting domain was solved numerically using the Euler method. The normal domain was not directly simulated and matched. Instead we used the phenomenological relations described in the previous subsection to set the boundary condition at the front. Parameters describing the numerical "experiment" were chosen to be: $\mu = 0$, $\nu = 5$, $\Gamma = 0$, and κ in the range from 0.01 to 0.1. Size of the system is $L_x/x^* = 200$. The boundary conditions are: the total flux $\Phi/\left(B^* x^{*2}\right)$ in the range 0.5 to 2.5, temperature of the cold superconductor $\theta_0 = 0.7, \theta(x = -200) = \theta(x = 200) = \theta_0$.The normal phase was not simulated since it can be integrated analytically. The transition to the normal state at depairing current was taken into account by holding constant the normal domain Joule heat dissipation Ξ_n for values in the range $5 \cdot 10^{-2}$ to 2.

The results of the numerical solution are presented in Figs. 6-7. The evolution of the magnetic induction is presented in Fig. 6 for the following values of the flux and heat diffusion constant: a) $\Phi = 0.5$, $\kappa = 0.1$, b) $\Phi = 0.5$, $\kappa = 0.01$, c) $\Phi = 2.4$, $\kappa = 0.05$. The value of Ξ_n was kept fixed at $\Xi_n = 0.5$. Different curves represent successive times with intervals of $\Delta t = 2.5\ t^*$ between them. Velocity of the sharp front is constant and is plotted

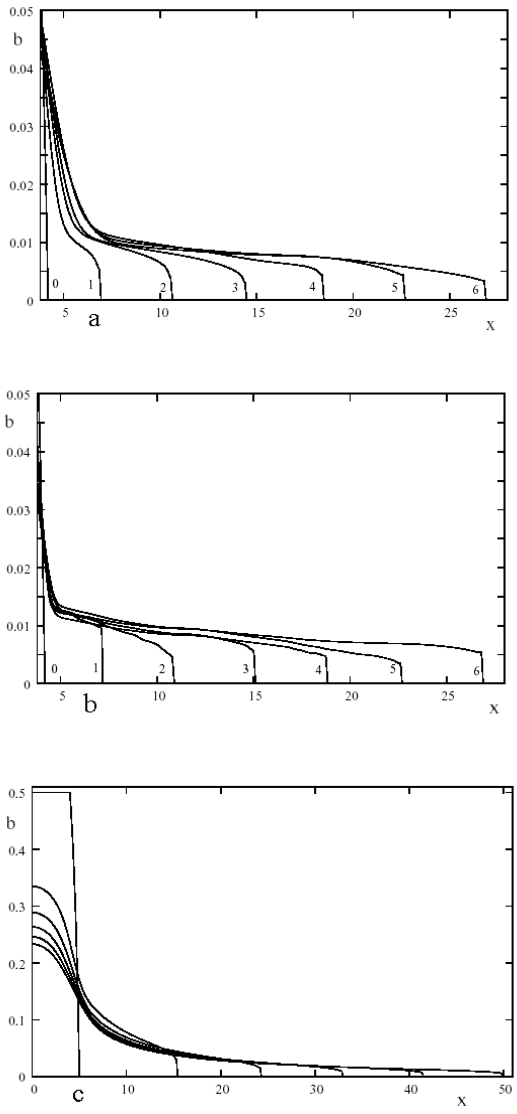

Figure 6: The evolution of the magnetic induction for the flux conserving boundary condition. The value of the Joule heat released in the normal domain.Ξ_n was kept fixed at $\Xi_n = 0.5$. The curves correspond (from left to right) to six different times with intervals of Δt between them. a) For the flux $\Phi = 0.5$ and the heat diffusion constant $\kappa = 0.1$, $\Delta t = 2.5\ t^*$, b) the same for $\Phi = 0.5$, $\kappa = 0.01$, $\Delta t = 2.5\ t^*$, c) $\Phi = 2.4$, $\kappa = 0.05$, $\Delta t = 5\ t^*$.

as function of Ξ_n in Fig. 6 for $\Phi = 2.4$ and $\kappa = 0.05$. The temperature front moves together with the flux front velocity. The time instants are the same as for the magnetic induction. It demonstrates that the front interface velocity V is linearly dependent on Ξ_n. The dependence on Φ is negligible. The results closely follow Eq.(39) obtained analytically for $\kappa = 0$ and confirm the general physical picture proposed in the previous section that the velocity of the shock wave is universal in a sense that it depends only on the heat released in the normal domain. The simulation reveals that the evolution is qualitatively the same for values of other parameters.

The dynamics of the temperature distribution $\theta(x,t)$ is presented in Fig. 7 and has a form of the thermal shock wave. Two sets of parameters were simulated: a) $\Phi = 0.5$, $\kappa = 0.1$, b) $\Phi = 0.5$, $\kappa = 0.01$. The maximum of temperature θ in this wave is reached at the interface between the superconducting and normal domains in the vicinity of the magnetic flux front. As we discussed in the previous section, the current is maximal in the normal domain which is narrow. In all the cases studied we found that the Joule heat released in the mixed state domain (see Fig. 5) does not exceed 1% of that in the normal domain.

4 Instability of the straight front

4.1 Linear stability analysis

Essential dependence of the front velocity on the Joule heat released near the interface might lead to instability of the straight front. Perturbations like a slight spatial distribution of the sample parameters (resistance, for example) can trigger the front instability. Keeping the normal resistivity in the form $\rho_n = \rho_0 + \rho_1\theta(x,t)$ we look for a solution of the corrugated front in the normal domain as:

$$\begin{aligned} b &= b_n(x - Vt) + \eta(x,y,t); \\ \theta &= \theta_n(x - Vt) + \zeta(x,y,t). \end{aligned} \tag{40}$$

The leading order solution β_n and θ_n for the set of basic equations Eqs. (12),(13) for $\rho_1 = 0$ were obtained in section 3, while corrections to the first order in ρ_1 will not be required in the stability analysis. The first order terms in perturbations η and ζ are:

$$\frac{\partial \eta}{\partial t} = \rho_n(\theta_n)\,\boldsymbol{\nabla}^2\eta + \rho_1\frac{\partial \theta_n}{\partial x}\frac{\partial \eta}{\partial x} + \rho_1\frac{\partial^2 b_n}{\partial x^2}\zeta + \rho_1\frac{\partial b_n}{\partial x}\frac{\partial \zeta}{\partial x}; \tag{41}$$

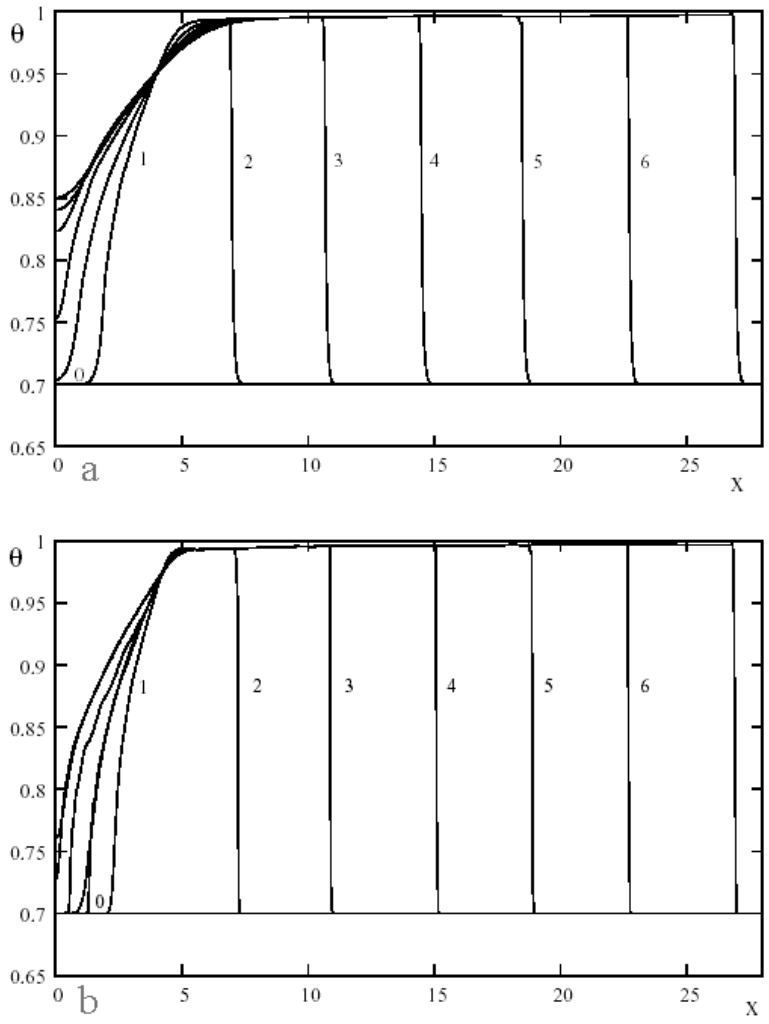

Figure 7: The evolution of the temperature profile for the flux conserving boundary condition. The value of the Joule heat released in the normal domain, Ξ_n, was kept fixed at $\Xi_n = 0.5$. The curves correspond to six different times with intervals of $\Delta t = 2.5\ t^*$ between them. a) For the flux $\Phi = 0.5$ and heat diffusion constant $\kappa = 0.1$, b) the same for $\Phi = 0.5$, $\kappa = 0.01$.

$$\frac{\partial \zeta}{\partial t} = 2\rho_n(\theta_n)\frac{\partial b_n}{\partial x}\frac{\partial \eta}{\partial x} + \rho_1\left(\frac{\partial b_n}{\partial x}\right)^2 \zeta. \tag{42}$$

Due to translation invariance of these eigenvalue equations in time and in the direction along the front y, one represents η, ζ in a form

$$\eta = \eta(x)\exp(\Omega t + k_y y);\ \zeta = \zeta(X)\exp(\Omega t + k_y y). \tag{43}$$

Then the eigenvalue equations become one-dimensional

$$\widehat{L}\begin{bmatrix} \eta \\ \zeta \end{bmatrix} = \Omega \begin{bmatrix} \eta \\ \zeta \end{bmatrix}, \tag{44}$$

where

$$\widehat{L} = \begin{array}{|c|c|} \hline \rho_n(\theta_n)\left(\frac{\partial^2}{\partial X^2} + \rho_1 \frac{\partial \theta_n}{\partial X}\frac{\partial}{\partial X} - k_y^2\right) & \rho_1\left(\frac{\partial b_n}{\partial X}\frac{\partial}{\partial X} + \frac{\partial^2 b_n}{\partial X^2}\right) \\ \hline 2\rho_n(\theta_n)\frac{\partial b_n}{\partial X}\frac{\partial}{\partial X} & \rho_1\left(\frac{\partial b_n}{\partial X}\right)^2 \\ \hline \end{array}. \tag{45}$$

Let us first consider a simpler case of conventional superconductors for which $\rho_1 = 0$. Substituting Eqs.(31)-(32) into Eqs.(41)-(42) one obtains (replacing $\frac{\partial}{\partial X} \to ik_X$):

$$\widehat{L}_0 = \begin{array}{|c|c|} \hline -\rho_0\left(k_X^2 + k_y^2\right) & 0 \\ \hline -2i\rho_0 j_d k_X & 0 \\ \hline \end{array}. \tag{46}$$

The matrix $\widehat{L}_0$ has one stable $\Omega_1 = -\rho_0\left(k_X^2 + k_y^2\right)$ and one marginal $\Omega_2 = 0$ eigenvalues. This eigenvalue is highly degenerate: any temperature deviation ζ for $\eta = 0$ belongs to this subspace: $\widehat{L}_0\begin{bmatrix} 0 \\ \zeta \end{bmatrix} = 0$. Strictly speaking, the marginal eigenvalue Ω_2 calls for investigation beyond the linear stability analysis. However, we believe it is stable and, in any case, addition of the ρ_1 term to resistivity removes the marginality and the degeneracy. To find the corrected eigenvalue Ω_2, one has to diagonalize on the corresponding subspace the operator:

$$\widehat{L}_{\zeta\zeta} = \rho_1\left(\frac{\partial b_n}{\partial X}\right)^2. \tag{47}$$

The derivative is nearly constant in the normal domain, see Eq.(31),

$$\widehat{L}_{\zeta\zeta} = \rho_1 j_{n0}^2 \exp\left[-\frac{2XV}{\rho_n}\right] \approx \rho_1 j_d^2. \tag{48}$$

Consequently

$$\Omega_2 = \rho_1 j_d^2, \tag{49}$$

which demonstrates the instability for any wave vector.

The physical reason for the instability is a positive feedback between temperature fluctuation at the front increasing, in its turn, both the Joule power at the front and its velocity. In fact, it is the well known hydrodynamic tangential instability of the flux front which is responsible for the front decomposition. Indeed, in this case warmer segments of the front move faster and might destroy the flat front line.

4.2 Stability in the general case. Numerical simulation

It should be noted that till now we have considered the $\kappa = \Gamma = 0$ case only. In this case the normal domain in the front shows instability in respect to small temperature fluctuations with arbitrary wave vectors. The dispersion appears for the non-zero heat diffusion coefficient. In fact, however, these small fluctuations cannot destroy the straight line front. It becomes unstable due to large amplitude fluctuations. Let us consider the evolution of the instability. First of all, the instability can develop when the characteristic time $t_0 \simeq 1/\left(\rho_1 j_d^2\right)$ is smaller than the characteristics time of the heat absorption in the sample $t_r \approx \Gamma^{-1}$. In addition, the heat diffusion along the y - axis can also affect the unstable fluctuations. In the later case the requirement is: $ut_0 > \sqrt{\kappa t_0}$. These two requirements allow us to determine the critical velocity of the fluctuation when the instability is developed:

$$u > u_c = \min\left\{\Gamma w_n, j_d\sqrt{\kappa\rho_1}\right\}. \tag{50}$$

In metals and alloys the normal state resistivity practically does not depend on temperature in the relevant temperature range. This means that $\rho_1 = 0$ and consequently no instability is expected. The threshold in the fluctuation velocity u_c (which is proportional to the Joule heat released in the front) means that only a large temperature fluctuation can provide essential Joule heat to destroy the front. Physically large amplitude fluctuations of the temperature at the front are non-uniform because they are caused by the spatial distribution of the impurities in the sample locally increasing resistivity and hence the Joule heat and velocity of the fluctuations in the front. Numerical analysis carried out in the present manuscript supports this scenario. In order to study the development of instability for arbitrary κ, the set of the Eqs. (12)-(13) have been solved numerically. The Joule heat power Ξ_n released in the normal domain at the front has the following model form:

$$\frac{\Xi_n(\theta)}{\Xi_{n0}} \equiv \frac{\rho_n(\theta)}{\rho_0} = 1 + \alpha\left[\theta(x,y,t) - \theta_0\right], \tag{51}$$

where initial temperature is perturbed along the y - axis (temperature fluctuation) $\theta(y, t = 0) = 0.88$ for $4 < y < 5$, while $\theta(y, t = 0) = \theta_0 = 0.7$ for y outside this interval. We chose $\alpha = 14.5$, $\kappa = 0.05$, and 2.5. Physically, this kind of fluctuation represents a local variation of the normal state resistivity (proportional to Ξ_n) when front of the shock wave passes an inhomogeneity.

The evolution of a small fluctuation in two opposite cases is presented in Fig. 8. For small κ, Fig. 8a, an unstable pattern of the magnetic induction develops. It should be noted that the flux front line lost its stability practically immediately after the temperature fluctuation affected the system. For finite κ we observe that most of the $\kappa = 0$ unstable modes are diffused away and do not develop into instability of the system. For large κ, Fig. 8b, a similar perturbation relaxes into a straight line front and disappears in accord with the stability analysis.

5 Discussion

To summarize, we considered the formation, stability, and evolution of unstable normal domain forced onto a type-II superconductor subjected to a weak magnetic field. On the microscopic time scale normal domain disintegrates into a network of the Abrikosov vortices. The resulting vortex cluster forms a moving elastic medium eventually escaping the sample. At this early stage the flux front is not particularly sharp. However, on the mesoscopic time scale, when dissipation controls the dynamics, a sharp flux front is formed. Strong screening currents significantly exceeding the critical current J_c flow in the mixed state. For such strong currents the vortex matter resistivity R has a form $R \propto B^\nu J^\mu$. We predict that when $\nu > 1$ both the moving flux and the temperature profile form a sharp singular shock waves. Strong screening currents in the vortex matter approaching the depairing current J_d cause destruction of superconductivity. An area of material adjacent to the interface between the Meissner state and the mixed state of the size (returning to dimensional units) $W_n = \dfrac{cB^* (1 - T_0/T_c)}{4\pi\nu J_d}$ becomes normal. Here $B^* = \sqrt{4\pi C T_c}$, C is the heat capacity, and T_0 is temperature of the cool superconductor. The stable superconductor - normal interface is formed due to combined effect of the nonlinear magnetic flux dynamics and thermal effects. The condition $\nu > 1$ is independent of μ and has the following physical meaning. It is well known that above the critical current resistivity is proportional to the number of vortices (the flux flow Bardeen-Stephen formula), $R \propto B$ ($\nu = 1$). The condition for formation of the

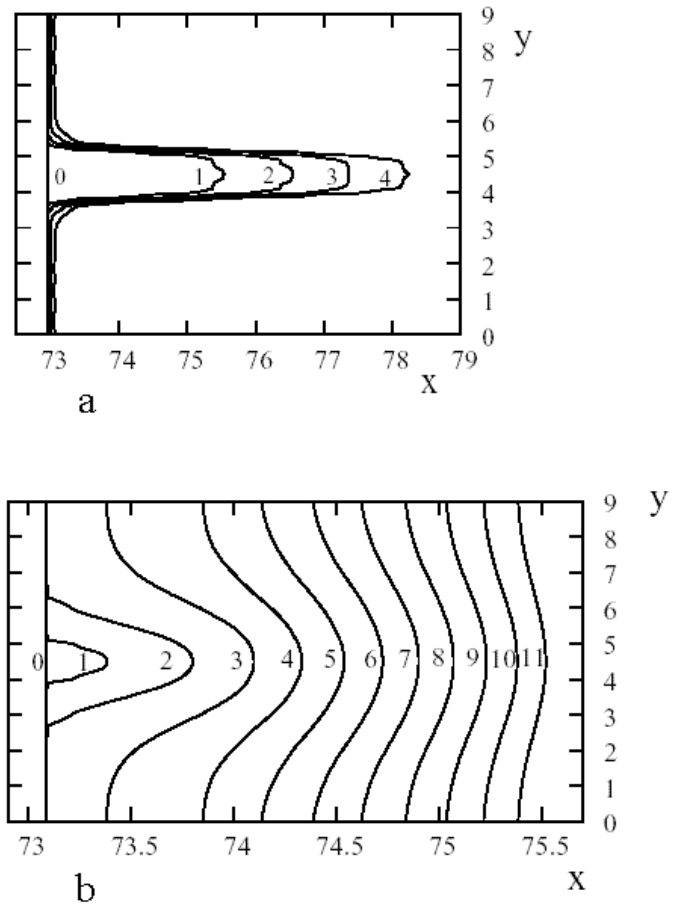

Figure 8: Evolution of the magnetic flux front pattern for different heat diffusion constants. The perturbation is triggered by the temperature inhomogeneity specified in Eq.(51). a) Small heat diffusion constant $\kappa = 0.05$. Development of the avalanche instability. Five snapshots (intervals of $\Delta t = 0.05\ t^*$) of a finger-shaped instability in magnetic induction are shown from left to right. b) Large heat diffusion constant $\kappa = 2.5$. Evolution of magnetic flux pattern. Five snapshots (intervals of $\Delta t = 0.125\ t^*$) show that the initially developed small fluctuation dissipates away.

normal domain is therefore that the dependence on magnetic induction at currents close to the depairing currents is stronger than linear. For Nb, this happens at least for small fields.

The interface moves with constant velocity, which is completely determined by the Joule heat released in the normal domain at the front and hence on the normal resistivity of the sample. The flux front velocity has the form for $\mu = 0$ (in dimensional units) $V = \dfrac{cR_n J_d}{(1 - T_0/T_c)\, B^*} \left(\dfrac{B^*}{B_{c2}\,(0)} \right)^{\nu}$. Taking, for example, material parameters of the optimally doped YBCO, $J_d = 10^8 \mathrm{A/cm}^2$, $R_n = 2 \cdot 10^{-6}$ Ω·cm, $C = 1$ J/cm^{3}K [8], one obtains for the flux front velocity $V \approx 10^5 \mathrm{cm/\,sec}$, which is in a good agreement with experimental data [6]. Note, however, that the value strongly depends on the exponents μ and ν. The width of the normal stripe is 0.5 μm.

The type of the voltage-current characteristic is therefore the decisive factor determining the flux front stability in type II superconductors. The instability is developed when the voltage-current characteristics of the uniform superconductor in its resistive state provides sufficient screening currents at the moving flux front interface. The physical reason for the instability is very similar to a well known hydrodynamic instability, when different layers of the liquid move with different and parallel velocities. In fact, it is the positive feedback between excessive local temperature at the front and Joule heat released there that leads to instability. The hydrodynamic tangential instability of the flux front destroys the flat front. The instability develops for the fluctuation velocities exceeding the critical value

$$U > U_c = \min \left\{ \frac{cB^*\,(1 - T_0/T_c)}{4\pi\nu J_d t_r}, \frac{J_d}{C} \sqrt{D\, \frac{dR_n}{dT}|_{T_c}} \right\},$$

where D is the heat diffusion constant and t_r is the heat absorption time. Taking $D = 30$ J/(cm sec K) and $t_r = 10^{-11}$ sec, one estimates the two velocities as $5 \cdot 10^6 \mathrm{cm/\,sec}$ and $2.6 \cdot 10^5 \mathrm{cm/sec}$.

The avalanche-type instability appears when moving flux front enters the area in which locally the normal resistivity is large. The experimental observation of the fast flux dynamics in YBCO has been carried out by Leiderer *et al.* [6]. The velocity of the front indeed has the universal character at the advanced stage of the instability and does not depend on initial magnetic gradients. Order of magnitude of the dendrite velocity on the later stages of disintegration of the front are expected to be of order of U_c. This instability is not expected to arise in materials like Nb since $\dfrac{dR_n}{dT}|_{T_c}$ is negligibly small and U_c vanishes.

We are grateful to D. Kessler, Y. Yeshurun, Y. Rabin, A. Shaulov, H.H. Wen for discussions, and V. Vinokur for his criticism. This work was supported by The Israel Science Foundation, ESF Program *Cosmology in the Laboratory*, and by the Heinrich Hertz Minerva Center for High Temperature Superconductivity. We are also grateful to the Binational Israel-USA and Germany-Israel Foundations for support and to the Inter-University Computational Center for providing Cray J932 supercomputer facilities. BR acknowledges support of NSC of ROC92-2112-M009-024 and hospitality in Bar Ilan University.

References

[1] R.G. Mints and A.I. Rahmanov, Rev. Mod. Phys. **53**, 551 (1981); A.V. Gurevich, R.G. Mints, and A.I. Rahmanov, *The Physics of Composite Superconductors* (Begell House, N.Y., 1997).

[2] L.A. Dorosinskii, M.V. Indenbom, V.I. Nikitenko, Yu.A. Ossipyan, A.A. Polanskii, and V.K. Vlasko-Vlasov, Physica C **203**, 149 (1992).

[3] T.H. Johansen, M. Baziljevich, H. Bratsberg, H. Hauglin, and G. Lafyatis, In: *High Temperature Superconductors: Synthesis, Processing, and Large-Scale Applications*, Ed. U. Balachandran, P.J. McGinn, and J.S. Abell, p.203 (The Minerals, Metals and Materials Society, 1996).

[4] C.A. Duran, P.L. Gammel, R.E. Miller, and D.J. Bishop, Phys. Rev. B **52**, 75 (1995).

[5] P. Leiderer, J. Boneberg, P. Brull, V. Bujok, and S. Herminghaus, Phys. Rev. Lett. **71**, 2646 (1993); U. Bolz, J. Eisenmenger, J. Schiessling, B-U. Runge, and P. Leiderer, Physica B **284-288**, 757 (2000); U. Bolz, D. Schmidt, B. Biehler, B-U.Runge, R.G. Mints, K. Numssen, H. Kinder, and P. Leiderer, Physica C **388-389**, 715 (2003).

[6] U. Bolz, B. Biehler, D Schmidt, B.U. Runge, and P. Leiderer, Europhys. Lett. **64**, 517-523 (2003).

[7] C. Villard, C. Peroz, and A. Sulpice, J. Low Temp. Phys. **131**, 957 (2003).

[8] M. Aravind and P.C.W. Fung, Meas. Sci. Technol. **10**, 979 (1999).